IMA Journal of Applied Mathematics (1986) **36**, 207–221

Reactive Infiltration Instabilities

J. CHADAM[1], D. HOFF[2], E. MERINO[1], P. ORTOLEVA[1], AND A. SEN[1]

[1]*Geo-Chem Research Associates, Inc., 400 East Third Street, Bloomington, Indiana 47401*

[2]*Mathematics Department, Indiana University, Bloomington, Indiana 47405*

[Received 17 June 1985 and in revised form 18 June 1986]

When a fluid flow is imposed on a porous medium, the infiltration flow may interact with the reaction-induced porosity variations within the medium and may lead to fingering instabilities. A nonlinear model of such interaction is developed and morphological instability of a planar dissolution front is demonstrated using a linear stability analysis of a moving-free-boundary problem. The fully nonlinear model is also examined numerically using finite-difference methods. The numerical simulations confirm the predictions of linear stability theory and, more importantly, reveal the growth of dissolution fingers that emerge as a result of these instabilities.

1. Introduction

IN recent years there has been much interest in reaction–transport systems that can self-organize macroscopic patterns.[4–9,11–13] The purpose of the present paper is to study the interaction of an imposed flow and reaction-induced porosity variations within a porous medium which may lead to morphological instabilities and develop into scalloped and fingered patterns within the medium. The main objective is to propose and demonstrate a mechanism for these fingering instabilities. We will refer to it as the porosity feedback mechanism and it operates as follows.

Consider a slab of porous medium between the spatial boundaries $z = 0$ and $z = L_z$. The slab is infinite in the x and y directions. We assume that it is initially filled with water which is in equilibrium with respect to the dissolution reactions. At time $t = 0$, water is imposed in the positive z direction and a pressure gradient is applied so that the pressure at $z = 0$ is greater than that at $z = L_z$. This pressure gradient induces a flow along the z direction. If the water imposed is undersaturated with respect to the porous medium, dissolution of the medium will commence. The dissolution is most rapid near $z = 0$ and slows down as z increases, since the water becomes saturated as it advances. With this the system may reach a state where the porosity becomes independent of the transverse position. We will call this the state of planar dissolution.

It can be easily seen that, under certain conditions the planar state may become unstable. Consider that in some region the porosity φ is slightly higher

Research supported by the U.S. Department of Energy, Office of Basic Energy Sciences, Engineering Research Program, Contract #DE-AC02-82ER12074

than elsewhere. Darcy's law states that the flow will be larger there since the permeability is an increasing function of the porosity. Increased flowthrough implies an increased rate of dissolution and hence a further increase in the local porosity, leading to a runaway effect. Thus the planar state may become unstable to perturbations that vary in the transverse direction.

The interaction of flow and dissolution in a porous medium is often extremely complicated, because of the presence of several soluble species (e.g. minerals) in the pores and many solute species in the fluid. In what follows, we first present a general macroscopic formulation of a model in which there is a single mineral in the medium. In our analytical studies we further restrict our attention to the simplified but generic situation of a single solute species. The present approach is based on the formulation of a moving-free-boundary problem[2,3,10,14]; we use the method of matched asymptotic expansions in the realistic limit case that the ratio, of the molar density of the solute to that of the solid mineral present in the medium, is very small. In typical rocks, this ratio may range from 10^{-3} to 10^{-10}. We perform a linear stability analysis[2,10] of a steady planar state in the above asymptotic limit. We find that disturbances having wavelengths larger than a critical value may become linearly unstable. This is followed by a numerical simulation of the full nonlinear problem. Our numerical computations clearly reveal the growth of dissolution fingers that emerge as a result of such morphological instabilities.

2. Equations of reactive infiltration

2.1 *General Macroscopic Formulation*

According to the scenario of the previous section, the interaction of flow and dissolution may destabilize the planar state. To describe this effect we will develop a simple model of the relevant processes. We introduce a set of macroscopic variables that are defined to have meaning in a statistical sense, i.e. they describe conditions in a volume element of space large enough to contain many grains or pores but shorter than the length scale of the phenomenon of interest. For self-consistency, the theory must predict patterns having length scales greater than a grain diameter.

Let $\mathcal{C} = (C_1, C_2, \ldots, C_N)$ be a listing of the concentrations (moles/rock volume) of the N chemical species in the fluid phase. Then conservation of mass yields

$$\frac{\partial \mathcal{C}}{\partial t} = -\nabla \cdot \mathcal{J} + \mathcal{R} \tag{2.1}$$

where J_i is the flux of species i and R_i is the source term due to dissolution (or precipitation) of the grains comprising the medium. In the present paper we assume that, with $C_i = \varphi c_i$,

$$J_i = -\varphi D_i(\varphi)\nabla c_i + \varphi c_i v \tag{2.2}$$

where φ is the porosity, i.e. the fraction of the medium that is pore space, and c_i is the concentration of the ith species in the pore space (i.e. moles per unit pore volume). Note that the diffusion coefficient $D_i(\varphi)$ of the ith species depends on φ. A common phenomonological relation for $D_i(\varphi)$ is [1]

$$D_i(\varphi) = \bar{D}_i \varphi^m \quad (\tfrac{3}{2} \leq m \leq \tfrac{5}{2}) \tag{2.3}$$

where $\bar{D}_i$ is a constant on the order of the diffusion coefficient of the ith species in water. We have neglected the effects of dispersion (the diffusion-like spreading of concentration gradients due to meandering and splitting of streamlines as the water flows around the grains [1]). This assumption is valid for slower flow speeds. Finally, the quantity $\boldsymbol{v}$ in equation (2.2) represents the fluid velocity.

We assume that, at time t in the vicinity of some point $\boldsymbol{r}$, the matrix is made up of soluble grains of local average volume $L^3(\boldsymbol{r}, t)$ and density $n(\boldsymbol{r})$. It also contains insoluble grains which occupy a volume fraction φ_n. Since nL^3 is the volume fraction occupied by the soluble grains, it follows that

$$nL^3 + \varphi + \varphi_n = 1. \tag{2.4}$$

If $G(n, L^3, \varsigma)$ is the rate of grain-volume change due to reaction, we have

$$\frac{\partial L^3}{\partial t} = G. \tag{2.5}$$

Hence (2.4) gives

$$\frac{\partial \varphi}{\partial t} = -nG \tag{2.6}$$

if the effect of nucleation is ignored ($\partial n/\partial t = 0$), since $\partial \varphi_n/\partial t = 0$ by definition of insolubility.

The rates R_i and G are related through stoichiometry. Assume that the solid dissolves according to the scheme

$$\text{Solid} \rightleftharpoons \sum_{i=1}^{N} \nu_i X_i$$

where X_i is the ith solute species in the pore fluid and ν_i is its stoichiometric coefficient. Let ρ be the molar density (moles/volume) of the soluble component. We may write

$$R_i = -\nu_i \rho n G;$$

the negative sign arises from the fact that the growth of crystals implies an uptake of solute species.

The density of water satisfies the conservation equation

$$\frac{\partial}{\partial t}(\varphi \rho_w) + \nabla \cdot (\varphi \rho_w \boldsymbol{v}) = 0, \tag{2.7}$$

$\varphi \rho_w$ being the density of water per unit rock volume.

Darcy's law relates the infiltration flow velocity v to the pressure gradient via the porosity-dependent permeability function $\kappa(\varphi)$; we have

$$v = -\kappa(\varphi)\nabla p.$$

A phenomological description of the permeability function $\kappa(\varphi)$ may be given by the so-called Fair–Hatch relation [1]

$$\kappa(\varphi) = \varphi^3/E_2[(1-\varphi)^{\frac{2}{3}} + E_1(\varphi_f - \varphi)^{\frac{2}{3}}]^2 \tag{2.8}$$

E_1 and E_2 being constants and $\varphi_f = 1 - \varphi_n$ is the final porosity. Since water has small compressibility and we neglect the dependence of ρ_w on the solute composition, ρ_w may be taken to be a constant. As a result, (2.7) becomes

$$\frac{\partial \varphi}{\partial t} = \nabla \cdot [\varphi \kappa(\varphi)\nabla p]. \tag{2.9}$$

Thus we have a closed set of equations (2.1, 2.6, 2.9) for the pore composition ζ, the porosity φ and the pressure p.

2.2 *Rate-Law Phenomenology*

An explicit expression for G is needed to complete the phenomenological description. We assume that G can be written as

$$G = kL^2\left(\prod_{i=1}^{N} c_i^{\nu_i} - K^{eq}\right) \tag{2.10}$$

where k is a rate coefficient and K^{eq} is the equilibrium constant. Thus $G = 0$ corresponds to a state of equilibrium (in the dilute solution approximation) and the rate increases with the surface area of the soluble grains, it being proportional to L^2. In view of (2.4), the rate law (2.10) takes the form

$$G = k\left(\frac{\varphi_f - \varphi}{n}\right)^{\frac{2}{3}}\left(\prod_{i=1}^{N} c_i^{\nu_i} - K^{eq}\right).$$

In setting forth this phenomenology, we have assumed that the time scale for diffusion to erase any compositional nonuniformity within a pore is much shorter than the rate of reaction or of flow through a pore, so that the concentration within a pore is a well-defined quantity.

2.3 *Boundary Conditions*

In our analytical treatment we shall examine an idealized problem of flow of water through a doubly infinite porous medium ($-\infty < z < \infty$). A flow from far left is imposed so that the condition

$$\nabla p \to p_f' z \quad \text{as} \quad z \to -\infty$$

applies, where p_f' is the pressure drop per unit length far upstream and z is a unit vector along the positive z axis, parallel to the imposed inlet flow. Because water

is incompressible and not consumed by the reaction, the pressure profile at $z \to +\infty$ is related to the initially given porosity and p_f'.

We assume that the inlet water is undersaturated with respect to the soluble component and hence have the condition that

$$c_i \to c_i^{\text{inlet}} \quad \text{as } z \to -\infty, \qquad \prod_{i=1}^{N} (c_i^{\text{inlet}})^{\nu_i} < K^{\text{eq}}.$$

The composition far to the right is assumed to have reached equilibrium and hence

$$c_i \to c_{i\infty} \quad \text{as } z \to \infty, \qquad \prod_{i=1}^{N} c_{i\infty}^{\nu_i} = K^{\text{eq}}.$$

Here $c_{i\infty}$ represents the concentration of the ith species far downstream (i.e. $z \to \infty$). Our problem is then to solve the equations (2.1, 2.6, 2.9) for ζ, φ, and p subject to some prescribed initial conditions and the above boundary conditions.

3. The planar state

3.1 *Statement of the Problem*

We now study the planar state of dissolution. We shall restrict ourselves to the problem of dissolution of a single-component solid and a single solute species with concentration c. For the planar state all quantities are independent of the transverse coordinates x and y, the overall flow being imposed in the z direction. The governing equations become

$$\frac{\partial}{\partial t}(\varphi c) = \frac{\partial}{\partial z}\left(\varphi D(\varphi)\frac{\partial c}{\partial z} + c\varphi\kappa(\varphi)\frac{\partial p}{\partial z}\right) - \rho k n^{\frac{1}{3}}(\varphi_f - \varphi)^{\frac{2}{3}}(c - c^{\text{eq}}), \quad (3.1a)$$

$$\frac{\partial \varphi}{\partial t} = -k n^{\frac{1}{3}}(\varphi_f - \varphi)^{\frac{2}{3}}(c - c^{\text{eq}}), \qquad \frac{\partial}{\partial z}\left(\varphi\kappa(\varphi)\frac{\partial p}{\partial z}\right) - \frac{\partial \varphi}{\partial t} = 0. \quad (3.1b,c)$$

These are subject to the boundary conditions

$$c \to c^{\text{eq}},\ \varphi \to \varphi_o \quad \text{as } z \to \infty; \qquad c \to 0,\ \varphi \to \varphi_f,\ \frac{\partial p}{\partial z} \to p_f' \quad \text{as } z \to -\infty. \quad (3.2)$$

Here we have used the more suggestive notation c^{eq} in place of K^{eq}; the final porosity φ_f is that left after the complete dissolution of the soluble component. The subscripts o and f in (3.2) and throughout the remainder of this paper refer to conditions far downstream and far upstream respectively.

3.2 *Constant-Velocity Dissolution Fronts*

The velocity of a planar front governed by the equations (3.1, 3.2) can be obtained as follows. We introduce a coordinate system (ζ, t) moving with the front by writing

$$\zeta = z - ut, \quad (3.3)$$

u being the velocity of the front. Then, from (3.1) the equations for a steady planar front can be written as

$$[\varphi D(\varphi)c' + c\varphi\kappa(\varphi)p' + u\varphi(c-\rho)]' = 0, \tag{3.4a}$$

$$u\varphi' - kn^{\frac{1}{3}}(\varphi_f - \varphi)^{\frac{1}{3}}(c - c^{eq}) = 0, \qquad [\varphi\kappa(\varphi)p' + u\varphi]' = 0, \tag{3.4b,c}$$

where a prime denotes d/dζ. These equations must be solved with the boundary conditions (3.2).

By integrating equations (3.4a,c) from $\zeta = -\infty$ to $\zeta = \infty$ and using the boundary conditions, we find

$$c^{eq}\varphi_o\kappa_o p_o' + u\varphi_o(c^{eq} - \rho) = -u\varphi_f\rho, \qquad \varphi_o\kappa_o p_o' + u\varphi_o = \varphi_f\kappa_f p_f' + u\varphi_f \tag{3.5}$$

which can be solved for the unknowns u and p_o', the pressure gradient far to the right. We have, from the first equation in (3.5), that

$$u = \frac{-\kappa_o p_o'}{1 + \rho(\varphi_f - \varphi_o)/c^{eq}\varphi_o}, \tag{3.6}$$

and eliminating u, we obtain

$$p_o' = \frac{\varphi_f\kappa_f[\varphi_o + (\rho/c^{eq})(\varphi_f - \varphi_o)]}{\varphi_o\kappa_o[\varphi_o + (\rho/c^{eq} - 1)(\varphi_f - \varphi_o)]}p_f'. \tag{3.7}$$

From Darcy's law, the flow-velocity at $z = -\infty$ ($+\infty$ respectively) is given by $v_f = -\kappa_f p_f'$ ($v_o = -\kappa_o p_o'$ respectively). In terms of these velocities, (3.5, 3.6) can be written

$$u = \frac{v_o}{1 + \rho(\varphi_f - \varphi_o)/c^{eq}\varphi_o}, \qquad v_o = \frac{\varphi_f[\varphi_o + (\rho/c^{eq})(\varphi_f - \varphi_o)]}{\varphi_o[\varphi_o + (\rho/c^{eq} - 1)(\varphi_f - \phi_o)]}v_f.$$

Since $\rho \gg c^{eq}$ we see that $u \ll v_o$ and

$$v_o \simeq (\varphi_f/\varphi_o)v_f \tag{3.8}$$

Since $\varphi_o < \varphi_f$, this last equation shows, as expected, that the infiltration flow in the altered zone is slower than that in the unaltered zone.

It is interesting to note that these results do not depend on the diffusion coefficient or the rate constant of the system. They are, in fact, a simple consequence of the overall reaction stoichiometry and the flow far from the zone where φ changes from φ_o to φ_f. This is different from reaction–diffusion waves, as in the Zhabotinsky reaction, where the speed depends on rate and transport coefficients. In either case, however, the wave profile depends strongly on these parameters.

4. Solid density asymptotics

4.1 *Formulation*

Generally speaking and particularly for minerals, the solid molar density ρ greatly exceeds the solute concentration. Thus it is appropriate to define a small

parameter

$$\varepsilon = c^{eq}/\rho \ll 1$$

and examine the limit $\varepsilon \to 0$. As mentioned in the introduction, a typical value of ε may range from 10^{-3} to 10^{-10}. In this asymptotic limit the region over which φ changes appreciably moves very slowly. Therefore we introduce a slow dimensionless time parameter τ defined by

$$t = (t^*/\varepsilon)\tau$$

with $t^* = (kn^{\frac{1}{3}}c^{eq})^{-1}$. The length, concentration, and pressure are scaled using the following dimensionless variables.

$$r = r^*\tilde{r}, \qquad c = c^{eq}\gamma, \qquad p = p^*\tilde{p},$$

where

$$r^* = [D(\varphi_f)t^*]^{\frac{1}{2}}, \qquad p^* = D(\varphi_f)/\kappa(\varphi_f).$$

For convenience, a dimensionless diffusion coefficient and a scaled permeability are defined as

$$D^*(\varphi) = D(\varphi)/D(\varphi_f) = (\varphi/\varphi_f)^m, \tag{4.0a}$$

$$\kappa^*(\varphi) = \frac{\kappa(\varphi)}{\kappa(\varphi_f)} = \left(\frac{(1-\varphi_f)^{\frac{2}{3}}}{(1-\varphi_f)^{\frac{2}{3}} + E_1(\varphi_f - \varphi)^{\frac{2}{3}}}\right)^2 \left(\frac{\varphi}{\varphi_f}\right)^3, \tag{4.0b}$$

where $\kappa(\varphi)$ is given by (2.8). The equations (2.1, 2.6, 2.9) can now be written in the following dimensionless form (after dropping the tildes on $\tilde{r}$ and $\tilde{p}$):

$$\varepsilon \frac{\partial}{\partial \tau}(\varphi\gamma) = \nabla \cdot (\Delta \nabla \gamma + \lambda \gamma \nabla p) + \frac{\partial \varphi}{\partial \tau}, \qquad \varepsilon \frac{\partial \varphi}{\partial \tau} = -(\varphi_f - \varphi)^{\frac{2}{3}}(\gamma - 1), \tag{4.1a,b}$$

$$\nabla \cdot (\lambda \nabla p) = -(\varphi_f - \varphi)^{\frac{2}{3}}(\gamma - 1). \tag{4.1c}$$

Here, $\Delta = \Delta(\varphi) = \varphi D^*(\varphi)$ and $\lambda = \lambda(\varphi) = \varphi\kappa^*(\varphi)$. These equations are subject to the dimensionless boundary conditions

$$\gamma \to 0, \quad \varphi \to \varphi_f, \quad \partial p/\partial z \to p_f' \qquad \text{as } z \to -\infty, \tag{4.2a}$$

$$\gamma \to 1, \quad \varphi \to \varphi_o, \quad \partial p/\partial z \to p_o' \qquad \text{as } z \to \infty, \tag{4.2b}$$

where φ_f, p_f', ϕ_o are given and p_o' must be determined.

4.2 *The Moving-Boundary Problem*

In the limit $\varepsilon \to 0$, equation (4.1b) yields

$$(\varphi_f - \varphi)^{\frac{2}{3}}(\gamma - 1) = 0.$$

Therefore either $\gamma = 1$ or $\varphi = \varphi_f$. If $\gamma = 1$, we find from equation (4.1c) that $\nabla \cdot (\lambda \nabla p) = 0$. Equation (4.1a) then shows that $\partial\varphi/\partial\tau = 0$, so that in the unaltered region where $\gamma = 1$ we must have $\varphi = \varphi_o$, its initial value. It follows that $\nabla^2 p = 0$ in this region. Similarly, in the altered region where $\varphi = \varphi_f$,

equation (3.1c) shows that $\nabla^2 p = 0$ must hold. Across the moving front, the porosity undergoes a jump from its initial value φ_o to its final value φ_f. We will denote the location of this moving interface by $S(\boldsymbol{r}, t) = 0$ so that $S > 0$ represents the unaltered and $S < 0$ the altered zones respectively. These considerations lead to the following Stefan moving-boundary problem. In the downstream region $S > 0$ we have

$$\varphi = \varphi_o, \qquad \nabla^2 p = 0, \qquad \gamma = 1 \tag{4.3}$$

whereas the upstream ($S < 0$) equations are

$$\varphi = \varphi_f, \qquad \nabla^2 p = 0, \qquad \nabla \cdot (\Delta_f \nabla \gamma + \lambda_f \gamma \nabla p) = 0 \tag{4.4}$$

where $\lambda_f = \lambda(\varphi_f) = \varphi_f$ and $\Delta_f = \Delta(\varphi_f) = \varphi_f$. Equation (4.4) is derived from (4.1a) using the fact that $\varphi = \varphi_f$ in the region $S < 0$.

Equations (4.3, 4.4) must be solved subject to the boundary conditions (4.2) and the following continuity and jump conditions across the moving interface $S = 0$.

$$\gamma(0-) = \gamma(0+), \qquad p(0-) = p(0+), \tag{4.5a,b}$$

$$\Delta_f \frac{\partial \gamma}{\partial n}(0-) = \mu(\varphi_f - \varphi_o), \qquad \frac{\partial p}{\partial n}(0-) = \beta \frac{\partial p}{\partial n}(0+). \tag{4.5c,d}$$

Here, μ is the normal advancement velocity of the front and

$$\beta = \varphi_o \kappa_o / \varphi_f \kappa_f. \tag{4.6}$$

The notations $0-$ and $0+$ have been used to indicate approaching the interface from the regions $S < 0$ and $S > 0$ respectively and $\partial/\partial n$ represents differentiation in a direction normal to the moving interface. The continuity and jump conditions (4.5) are derived in detail in the Appendix. The conditions (4.5a,b) indicate that both concentration and pressure are continuous across the interface $S = 0$ whereas the jump in the concentration gradient across the interface is related to the normal advancement velocity μ according to (4.5c). Finally, the jump in the pressure gradient across the interface is given by (4.5d). These equations must be augmented by the kinematic condition, namely

$$\frac{\partial S}{\partial \tau} + \mu |\nabla S| = 0. \tag{4.7}$$

4.3 *The Planar State*

In the limit of large solid density ($\varepsilon \to 0$) the profiles of concentration and pressure can be easily derived. Denoting the planar quantities with an overbar and writing $\zeta = z - \bar{\mu}\tau$, we obtain

$$\bar{\gamma}(\zeta) = \begin{cases} 1 & \text{if } \zeta > 0, \\ \exp(\alpha\zeta) & \text{if } \zeta < 0, \end{cases} \qquad \bar{p}(\zeta) = \begin{cases} p_o' \zeta & \text{if } \zeta > 0, \\ p_f' \zeta & \text{if } \zeta < 0, \end{cases}$$

where $p_f' = \beta p_o'$ and $v_o = -\kappa_o p_o'$; the quantity α has the definition $\alpha = -p_f'$ and β

is defined in equation (4.6). This defines p_o' in terms of φ_o, φ_f, and p_f' and agrees with equation (3.8). The advancement velocity of the planar front is found from (4.7) to be

$$\bar{\mu} = -\varphi_f p_f'/(\varphi_f - \varphi_o).$$

4.4 *Linear Stability Analysis*

We now consider small time-dependent perturbations on the planar state by writing

$$S(y, \tau) = \zeta + \delta\psi(y, \tau), \tag{4.8a}$$

$$p(y, \zeta, \tau) = \bar{p}(\zeta) + \delta\hat{p}(\zeta)\psi, \qquad \gamma(y, \zeta, \tau) = \bar{\gamma}(\zeta) + \delta\hat{\gamma}(\zeta)\psi, \tag{4.8b,c}$$

with

$$\psi(y, \tau) = \exp \omega\tau \cos my. \tag{4.8d}$$

Here m is the wavenumber, δ is the amplitude ($\delta \ll 1$), and ω is the rate of growth of the perturbations ($\omega < 0$ signifying decay). Note that, in the limit $\varepsilon \to 0$, the porosities on either side of the front must remain unperturbed at their steady planar values φ_o and φ_f. Furthermore, the concentration γ remains unperturbed ahead of the front. Substituting the expansions (4.8) in (4.3, 4.4) we find that the variables $\hat{p}(\zeta)$ and $\hat{\gamma}(\zeta)$ satisfy the equations

$$\frac{d^2\hat{p}}{d\zeta^2} - m^2\hat{p} = \begin{cases} -m^2 p_f' & \text{if } \zeta < 0, \\ -m^2 p_o' & \text{if } \zeta > 0, \end{cases}$$

$$\frac{d^2\hat{\gamma}}{d\zeta^2} - \alpha\frac{d\hat{\gamma}}{d\zeta} - m^2\hat{\gamma} = -m^2\alpha e^{\alpha\zeta} - \alpha\beta\frac{d\hat{p}}{d\zeta}e^{\alpha\zeta} \quad (\zeta < 0), \qquad \hat{\gamma} = 0 \quad (\zeta > 0). \tag{4.9}$$

These must be solved subject to the boundary conditions

$$\hat{p}(-\infty) = \hat{p}(\infty) = \hat{\gamma}(-\infty) = 0$$

and the continuity and jump conditions

$$\hat{\gamma}(0) = -\alpha, \qquad \hat{p}(0-) = \hat{p}(0+) + (1-\beta)p_o'.$$

The kinematic condition (4.7) yields

$$\frac{\partial\psi}{\partial\tau} = \frac{\Delta_f}{\varphi_f - \varphi_o}\left(\frac{\partial\hat{\gamma}}{\partial n}(0-) + \alpha^2\psi\right). \tag{4.10}$$

Clearly, $\hat{p}$ is given by

$$\hat{p} = \begin{cases} p_f' + \beta\Lambda \exp(m\zeta) & \text{if } \zeta < 0, \\ p_o' - \Lambda \exp(-m\zeta) & \text{if } \zeta > 0, \end{cases} \tag{4.11}$$

where $\Lambda = 2(1-\beta)p_o'/(1+\beta)$. We now substitute the results (4.11) in equation (4.9), and solve for $\hat{\gamma}$ using the appropriate boundary, continuity, and jump conditions. Then, using the kinematic condition (4.10), we obtain the dispersion

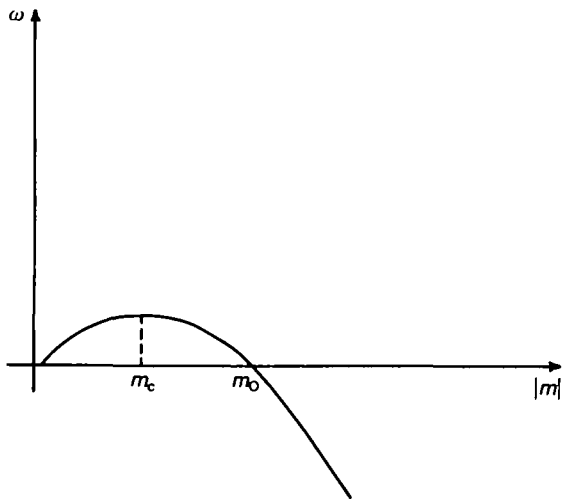

FIG. 1. Dependence of the stability eigenvalue ω on wavenumber m for small perturbations from the planar dissolution interface.

relation

$$\omega(m) = \frac{2\varphi_0 v_0}{(1+\beta)(\varphi_f - \varphi_0)}[\alpha + (1-\beta)|m| - (\alpha^2 + 4m^2)^{\frac{1}{2}}].$$

The dependence of the growth rate ω on the wavenumber m is shown in Fig. 1.

An analysis of Fig. 1 shows the nature of the morphological instability of the planar state. For small m (long wavelengths) we find

$$\omega = \frac{2\varphi_0 v_0(1-\beta)}{(\varphi_f - \varphi_0)(1+\beta)}|m|.$$

Since $\beta < 1$, it is clear that ω is positive for small m and hence the system is unstable to long-wavelength perturbations. (The fact that $\omega \to 0$ as $m \to 0$ is a direct consequence of the translational invariance of the system.)

For large m, it can easily be shown that

$$\omega = \frac{-2\varphi_0 v_0}{\varphi_f - \varphi_0}|m|$$

and therefore the system is stable to short-wavelength perturbations. Hence there exists a cut-off wavenumber, denoted by m_0, such that $\omega(m_0) = 0$. We find

$$m_0 = \frac{2(1-\beta)\alpha}{(3-\beta)(1+\beta)}.$$

As seen from Fig. 1, there is a value of $m = m_c$ at which ω reaches a maximum;

$$m_c = \frac{(1-\beta)\alpha}{2[(3-\beta)(1+\beta)]^{\frac{1}{2}}}.$$

The maximum amplification rate is given by

$$\omega_c = \frac{2 - [(3-\beta)(1+\beta)]^{\frac{1}{2}}}{(\varphi_f - \varphi_o)(1-\beta)} \alpha^2 \Delta_f.$$

5. Numerical simulation of porosity fingering

The fully nonlinear problem for the development of a nonplanar dissolution interface is investigated numerically in a rectangular domain (see Fig. 2) using a finite-difference scheme. The equations (4.1) are solved (with a finite value of ε) subject to the following boundary and initial conditions. No-flux conditions are used at the upper and lower boundaries so that

$$\partial p/\partial y = \partial \gamma/\partial y = 0 \quad (y = 0, L_y).$$

At the right wall it is appropriate to use the conditions

$$p = p_R(y), \quad \partial \gamma/\partial z = 0 \qquad (z = L_z),$$

where $p_R(y)$ represents the pressure level prescribed at the right wall. In our computations we have taken $p_R(y) = 0$. The value of the inlet concentration is taken to be zero while the inlet flow velocity v_f is prescribed. Thus we have

$$\gamma = 0, \quad \partial p/\partial z = -v_f/\kappa_f \qquad (z = 0).$$

The initial conditions for the concentration and porosity are chosen as follows.

$$\varphi(y, z, 0) = \varphi_o + (\varphi_f - \varphi_o)e^{-\xi}, \qquad \gamma(y, z, 0) = (1 - e^{-z/\delta})(1 - e^{-\xi}), \quad (5.1a,b)$$

with

$$\xi(y, z) = (y^4 + z^4)/(wL_y)^4. \qquad (5.1c)$$

The conditions (5.1a,b) are appropriate for testing the evolution of a small finger in the front near the corner $y = z = 0$. In this corner the porosity is near its post-washout value φ_f, the porosity being its initial value φ_o elsewhere. The initial finger is of length wL_y (with $w < 1$) and width $2wL_y$. Note that we have used the condition of symmetry about the side $y = 0$, i.e.

$$\partial p/\partial y = \partial \gamma/\partial y = 0 \quad (y = 0),$$

so that the total width of the rectangular channel is $2L_y$. The factor δ appearing in (5.1b) allows us to prescribe initial data that are not too stiff. A typical value of δ used in the numerical computations is 0·2.

Our numerical scheme may be described as follows. Denote the approximation to $\varphi(k\Delta y, l\Delta z, n\Delta t)$ by φ_{kl}^n; similarly γ_{kl}^n and p_{kl}^n for the concentration and pressure respectively. Computations are carried out in the rectangular domain shown in Fig. 2 with $L_y = 2$, $L_z = 8$ and 12. Typical values of Δy, Δz, and Δt are 0·2, 0·4, and 0·01 respectively. Equation (4.0) is used for the scaled permeability function with $E_1 = 1$ and for the scaled diffusion coefficient with $m = 2$. Given φ_{kl}^n, γ_{kl}^n, and p_{kl}^n at all the grid points in the rectangle, the computations of φ_{kl}^{n+1}, γ_{kl}^{n+1}, and p_{kl}^{n+1} are carried out as follows.

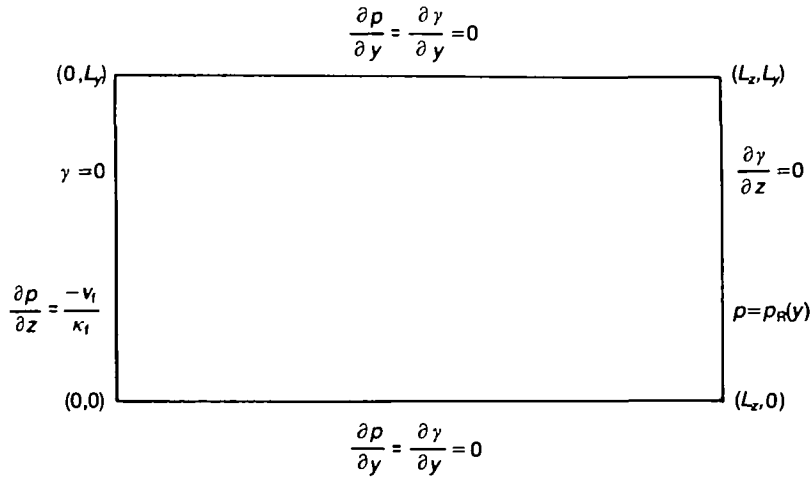

FIG. 2. Domain in which numerical simulation of the reactive percolation equations is carried out. Note that in view of the reflection symmetry about the $y = 0$ axis, the numerical solutions should be interpreted in a domain twice as large in the y-direction, the physical domain being $-L_y \leqslant y \leqslant +L_y$.

The approximation φ_{kl}^{n+1} is obtained by applying at each grid point the modified Euler method to (4.1b) with γ evaluated at time $n\Delta t$. This scheme is selected because it exhibits absolute stability for any choice of Δt. The resulting implicit equations are solved iteratively making sure the computed values of φ remain in the invariant interval $[\varphi_0, \varphi_f]$.

The value of γ_{kl}^{n+1} is computed by applying an operator-splitting version of the standard implicit finite-difference scheme to (4.1a). The pressure p is evaluated at time $n\Delta t$ and φ at time $(n+1)\Delta t$. This results in two tridiagonal systems of equations which are solved at each time step. Again, the fully implicit differencing insures unconditional stability and the computations are arranged so that the values of γ computed remain in the invariant interval $[0, 1]$.

For the computation of pressure p_{kl}^{n+1}, a central-difference scheme is used on (4.1c) with φ and γ evaluated at time $(n+1)\Delta t$. The resulting linear equations are solved using the method of successive overrelaxation.

The numerical results are presented in Figs 3–5 as a series of porosity contours at various times. The specific parameter values used in the computation are given in the figure captions. The inlet flow velocity, which in turn is determined by the

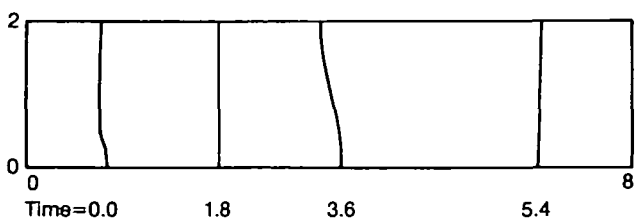

FIG. 3. Temporal sequence of porosity contours for a stable system. The parameter values used are: $\varphi_0 = 0{\cdot}1$, $\varphi_f = 0{\cdot}2$, $c^{eq}/\rho = 0{\cdot}05$, $p_f' = -1$. The figure shows porosity contours with $\varphi = 0{\cdot}15$.

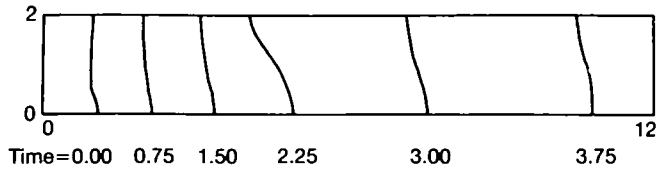

FIG. 4. Temporal sequence of porosity contours with $\varphi = 0{\cdot}15$ for an unstable system. The parameter values used here are the same as those in Fig. 3 except that $p_f' = -2$.

upstream pressure gradient, is used as the controlling parameter for studying the stability. As described earlier in this section, the initial state is taken to be a planar front with a small bump near the lower left corner. In Fig. 3, the inlet velocity is prescribed at a value which leads to a stable situation. This figure clearly shows that as the front (which was initially planar except for a small bump in the lower left corner) advances, it attains a planar shape after sufficient time has elapsed. The situation in Fig. 4 corresponds to an unstable state. Here the inlet velocity exceeds its critical value. Note that the bump now grows to a favoured amplitude and shape and then, having attained this new stabilized form, moves down the channel with a constant velocity. A highly unstable state of the system, giving rise to an elongated finger, is shown in Fig. 5.

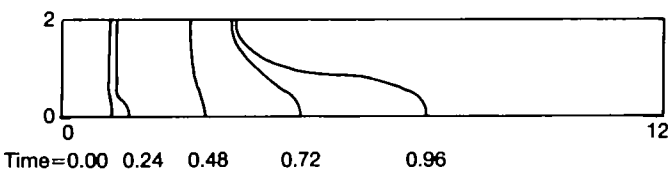

FIG. 5. Temporal sequence of porosity contours with $\varphi = 0{\cdot}15$ for a highly unstable system. Same parameter values as in Fig. 3 are used here except that now for $p_f' = -10$.

Appendix: Derivation of continuity and jump conditions

The boundary conditions at the moving interface $S(\boldsymbol{r}, t) = 0$ can be derived by analysing the small-scale structure of the transition layer around the interface. For this purpose we will use the method of matched asymptotic expansions in the limit of large solid density ($\varepsilon \to 0$) and study spatial variations normal to the interface on a length scale of $O(\varepsilon^{\frac{1}{2}})$. Let $\boldsymbol{r}_s(t)$ be a point on the interface. It is convenient to use a coordinate system moving with $\boldsymbol{r}_s(t)$ at its centre. Let σ denote a coordinate normal to $S = 0$, and $\boldsymbol{r}^*$ a coordinate in the plane tangent to $S = 0$ at $\boldsymbol{r}_s(t)$. In these new coordinates we have

$$[\nabla]_\tau = \boldsymbol{n}\frac{\partial}{\partial \sigma} + \nabla$$

where $\boldsymbol{n}$ is a unit normal at $S = 0$, i.e.

$$\boldsymbol{n} = \nabla S/|\nabla S|,$$

and ∇^* is the two-dimensional gradient operator in the tangent plane. Further,

$$\left[\frac{\partial}{\partial\tau}\right]_r = \left[\frac{\partial}{\partial\tau}\right]_{\sigma,r^*} - \frac{d\boldsymbol{r}_s}{d\tau}\cdot\left(\boldsymbol{n}\frac{\partial}{\partial\sigma} + \nabla^*\right).$$

But since the surface $S = 0$ advances along its normal with a velocity μ, say. It follows that $d\boldsymbol{r}_s/dt = \boldsymbol{n}\mu$ and therefore

$$\left[\frac{\partial}{\partial\tau}\right]_r = \left[\frac{\partial}{\partial\tau}\right]_{\sigma,r^*} - \left[\mu\frac{\partial}{\partial\sigma}\right]_{\tau,r^*}.$$

These relations may be used to transform the equations of motion (4.1) into the form relative to the frame that is stationary with respect to the moving interface. Considering all quantities to be functions of σ, $\boldsymbol{r}^*$, and τ, we obtain

$$\varepsilon\left(\frac{\partial}{\partial\tau} - \mu\frac{\partial}{\partial\sigma}\right)(\varphi\gamma) = \nabla\cdot[\Delta(\varphi)\nabla\gamma + \varphi\gamma\kappa\nabla p] + \left(\frac{\partial}{\partial\tau} - \mu\frac{\partial}{\partial\sigma}\right)\varphi, \qquad \text{(A.1a)}$$

$$\varepsilon\left(\frac{\partial}{\partial\tau} - \mu\frac{\partial}{\partial\sigma}\right)\varphi = -(\varphi_t - \varphi)^{\frac{1}{3}}(\gamma - 1), \qquad \nabla\cdot(\lambda\nabla p) = \varepsilon\left(\frac{\partial}{\partial\tau} - \mu\frac{\partial}{\partial\sigma}\right)\varphi. \qquad \text{(A.1b,c)}$$

In order to derive the continuity and jump conditions across the interface, we expand all quantities in powers of $\varepsilon^{\frac{1}{2}}$ by writing

$$p = p_0 + \varepsilon^{\frac{1}{2}}p_1 + \cdots, \qquad \varphi = \varphi_0 + \varepsilon^{\frac{1}{2}}\varphi_1 + \cdots,$$
$$\gamma = \gamma_0 + \varepsilon^{\frac{1}{2}}\gamma_1 + \cdots, \qquad \mu = \mu_0 + \varepsilon^{\frac{1}{2}}\mu_1 + \cdots.$$

For the 'inner' behaviour within the interface (i.e. for small σ), we consider the above variables to be functions of $\boldsymbol{r}^*$ and a short-distance variable ξ defined by $\xi = \varepsilon^{-\frac{1}{2}}\sigma$. If we insert these expansions in equations (A.1) and collect terms to various orders in $\varepsilon^{\frac{1}{2}}$, we find, to leading order, the equations

$$\frac{\partial}{\partial\xi}\left(\Delta(\varphi_0)\frac{\partial\gamma_0}{\partial\xi} + \varphi_0\gamma_0\kappa(\varphi_0)\frac{\partial p_0}{\partial\xi}\right) = 0, \qquad \frac{\partial}{\partial\xi}\left(\varphi_0\kappa(\varphi_0)\frac{\partial p}{\partial\xi}\right) = 0. \qquad \text{(A.2a,b)}$$

The last equation shows that $\varphi_0\kappa(\varphi_0)\dfrac{\partial p_0}{\partial\xi}$ is constant throughout the interfacial region. But away from the interface ($|\xi|\to\infty$), pressure is a smooth function (satisfying $\nabla^2 p = 0$) and hence $\partial p/\partial\xi \to 0$ as $|\xi|\to\infty$. Therefore the value of this constant must be zero. Since φ_0 and $\kappa(\varphi_0)$ do not vanish at the interface, it follows that

$$\frac{\partial p_0}{\partial\xi} = 0.$$

Thus p_0 remains continuous across the interface $S = 0$ and we have the condition (4.5b). Using this in (A.2a), it can be easily deduced that γ_0 is also continuous across the interface, so that the condition (4.5a) holds.

At the next order, equations (A.1a,c) give

$$\frac{\partial}{\partial \xi}\left(\Delta(\varphi_0)\frac{\partial \gamma_1}{\partial \xi} + \varphi_0\gamma_0\kappa(\varphi_0)\frac{\partial p_1}{\partial \xi} - \mu_0\varphi_0\right) = 0,$$
$$\frac{\partial}{\partial \xi}\left(\varphi_0\kappa(\varphi_0)\frac{\partial p_1}{\partial \xi}\right) = 0. \qquad \text{(A.3a,b)}$$

We now invoke the following matching conditions. Note that the normal derivative $\boldsymbol{n}\cdot\nabla$ at the surface $S=0$ is simply $\partial/\partial\sigma$. Matching the outer limit of the derivative of the inner solution ($|\xi|\to\infty$) with the inner limit of the derivative of the outer solution ($S\to 0\pm$) we have the condition

$$\lim_{S\to 0\pm} \vec{n}\cdot\vec{\nabla}p_0 = \lim_{\xi\to\pm\infty}\frac{\partial p_1}{\partial \xi}. \qquad \text{(A.4)}$$

Combining (A.4) with the integral from $\xi=-\infty$ to $\xi=+\infty$ of (A.3b), we find that the jump in the pressure gradient across the interface is given by the condition (4.5d). Similarly, equation (A.3a) can be used to show that the concentration gradient also suffers a jump across the interface $S=0$, the magnitude of the jump being related to the advancement velocity μ, according to (4.5c).

References

1. Bear, J., 1972 *Dynamics of Fluids in Porous Media.* Amsterdam: Elsevier.
2. Chadam, J., & Ortoleva, P. 1983 The stabilizing effect of surface tension on the development of the free boundary in a planar, one-dimensional, Cauchy–Stefan problem, *IMA J. Appl. Math.* **30,** 57–66.
3. Friedman, A., 1984 *Partial Differential Equations of Parabolic Type.* Englewood Cliffs: Prentice-Hall.
4. Haase, S., Feinn, D., Chadam, J., & Ortoleva, P. 1980 Oscillatory zoning in plagioclase feldspar. *Science* **209,** 272–274.
5. Hedges, E., & Myers, J. E. 1926 *The Problem of Physico-Chemical Periodicity.* New York: Longmans-Green.
6. Liesegang, R. 1913 *Geologische Diffusionen.* Dresden and Leipzig: Steinkopff.
7. Merino, E., Ortoleva, P., & Strickholm, P. 1983 A kinetic theory of stylolite generation and spacing, *Min. and Pet.* **2,** 360–370.
8. Nicolis, G., & Prigogine, I. 1977 *Self Organization in Nonequilibrium Systems.* New York: Wiley.
9. Noyes, R. M., & McBirney, A. R. 1979 Crystallization layering of the Skaergoaand intrusions. *J. Petrology* **20,** 487–554.
10. Ockendon, J. 1980 Linear and nonlinear stability of a class of moving boundary problems. *1979 Paiva Seminar on Free Boundary Problems* (E. Magenese, ed.). Inst. Naz. di Aeta Mat., Rome.
11. Ortoleva, P. 1978 In: *Selected Topics from the Theory of Nonlinear Physico-Chemical Phenomena* (H. Eyring, Ed.), Vol. 4. Academic Press.
12. Ortoleva, P. 1979 The multifaceted family of the nonlinear: waves and fields, center dynamics catastrophes, rock bands and precipitation patterns. *1978 Bordeaux Conference on Far From Equilibrium Phenomena.* Springer-Verlag.
13. Ortoleva, P., Merino, E., & Strickholm, P. The self organization of metamorphic layering. *J. Geophys. Res.* (submitted for publication).
14. Rubenstein, L., 1971 *The Stefan Problem.* Vol. 27, Translations of Mathematical Monographs. AMS, Providence.